Research Paper

Exergy analysis and entropy generation of a reciprocating compressor applied in CNG stations carried out on the basis models of ideal and real gas

Amir Niazmand [a], Mahmood Farzaneh-Gord [a], Mahdi Deymi-Dashtebayaz [b,*]

[a] The Faculty of Mechanical Engineering, Shahrood University of Technology, Shahrood, Iran
[b] Faculty Member of Mechanical Engineering, Hakim Sabzevari University, Sabzevar, Iran

HIGHLIGHTS

- Surveying effects of key design factors on efficiencies of reciprocating compressor.
- Applying ideal gas and AGA8 equations of state for modeling.
- Attaining numerically trends of various entropy terms verse to crank angle.
- Studying effects of clearance, pressure ratio and angular speed on efficiencies.

ARTICLE INFO

ABSTRACT

In this work, a numerical analysis for observing the proficiency of reciprocating compressors used in CNG (Compressed Natural Gas) stations is studied thermodynamically for ideal model and real one. AGA8 state equation is intended for modeling real gas. The analysis is carried out on the basis of the entropy concept. To investigate effects of important design factors on entropy generation, isentropic and exergy efficiencies, a numerical method is developed. The considered design factors are clearance, angular speed, pressure ratio and input and output valve areas. In this analysis, the compressor cylinder is presumed as control volume, and methane is also chosen as the natural gas and modeled as both an ideal gas and real one. The results highlight that with increasing angular speed, entropy generating increases and consequently exergy and isentropic efficiencies decrease, while increase in clearance acquires the inverse results. Furthermore, it will reach to higher efficiency, if input valve area is considered more than output valve area. For instance, with choosing a suitable proportion, efficiency can increase as much as 6.47%.

1. Introduction

Reciprocating compressor type is employed in lots of industries such as gas transmission pipelines petrochemical plants and refineries. They are machines that have positive displacement. With converting rotating motion of crank to reciprocating displacement of piston, they cause working fluid compress and displace. To deliver gases at high pressure reciprocating one is a really suitable choice. This type of compressors has many advantages, such as (1) simplicity of the principle; (2) acceptance of wide variations in input and output conditions and (3) achieve a high compression ratio [1].

Using in CNG (Compressed Natural Gas) stations to compress gas is an outstanding application of reciprocating ones. In CNG stations, compressors, which are three or four stages, are applied to compress the gas from a low pressure (about 0.5 MPa) to a much more amount (20 MPa to 25 MPa) [2,3]. A substantial part of initial investment and maintenance costs of these stations are related to this type of compressor. In addition, relatively high power consumption is another main problem of this compressor type in CNG stations [3]. As regard to being worth fuels, an accurate simulation of the related compressors could ameliorate design parameters so as to enhance efficiency and subsequently reduce power consumption.

The reciprocating compressor type has been investigated extensively to modify their performance. For predicting the correct estimate of thermodynamic properties into cylinder such as in-cylinder temperature, pressure, motions of valves and mass in the completed compressor cycle, a few models were investigated

Nomenclature

a	lengths of rod (m)	Ve	velocity (m/s)
A	area (m^2)	W	actual work (kJ/kg)
C_d	orifice discharge coefficient	$\dot{W}$	actual work rate (kW or MW)
c_p, c_v	constant pressure & volume specific heats (kJ/kg K)	x	displacement (m)
D	diameter (m)	z	height (m)
g	gravitational acceleration (m/s^2)	ρ	density (kg/m^3)
h	specific enthalpy (kJ/kg)	ω	angular speed (rad/s)
L	crank [m]	α	heat transfer coefficient (W m^2/K)
$\dot{m}$	mass flow rate (kg/s)	θ	Degree (deg)
M	Molecular weight (kg/kmol)		
P	pressure (bar or Pa)	*Subscript*	
$\dot{Q}$	heat transfer rate (kW)	d	discharge condition
St	stroke (m)	cv	control volume condition
S	entropy (kJ/K)	ex	exergy
T	Temperature (K or °C)	gen	generation
t	time (s)	isen	isentropic
u	internal energy (kJ/kg)	ref	reference
v	specific volume (m^3/kg)	s	suction condition
V	volume (m^3)	p	piston
V_0	dead volume (m^3)	0	ambient

[4–8]. In one research, a universal method so as to study reciprocating compressors proficiency was presented by Stouffs et al. [4]. In another study, for predicting power consumption and the thermodynamic factors of this compressor type during compression process, a numerical simulation was presented by Damle et al. [5]. A comprehensive numerical model of fluid dynamic and thermal demeanour related to reciprocating compressors was also developed by Farzaneh-Gord et al. [7], which is employed in CNG stations. Besides this, the special effects of described design factors on the requisite work used for compressing gas, and variations of in-cylinder thermodynamic properties have been observed too. Furthermore, Farzaneh-Gord et al. [8] investigated the influences of compositions of different natural gas on proficiency of reciprocating type of compressor with using a numerical model. This model could predict compressor parameters such as pressure, temperature, required work mass flow rate, mass and displacement of valves.

Concentrating on proficiency of the reciprocating ones is also another subject which has been regarded in many studies. In one study, considered exploration of reciprocating ones through computational fluid dynamics was deliberated by Pereira et al. [9]. They employed a three-dimensional formulation for analyzing geometries of actual discharge and suction muffler with using a suitable model. They validated their numerical values with experimental results such as valve displacement and pressure in the input and compression chambers obtained in a calorimeter facility. A detailed simulation with considering various thermodynamic efficiencies of the reciprocating ones was developed by Pérez-Segarra et al. [10]. In this work, different efficiencies such as volumetric efficiency, isentropic efficiency and combined mechanical-electrical efficiency were employed and divided into several partial efficiencies into identify influences of various physical subprocesses. Besides this, Casting et al. [11] proposed a dynamic pattern so as to simulating reciprocating compressor type, and they then validated numerical results with experimental values. Their results illustrate that clearance (ratio of dead volume) and a factor related to friction have significant effects on volumetric efficiency and effective efficiencies in turn. By using energy and mass balances, and compared these results to experimental data for compressors, a numerical investigation was presented by Porkhial et al. [12]. Aprea and Renno [13] proposed an experimental model

for determining the optimum frequency at each working condition, and then the related energy saving associated with that choice. Tang Bin et al. [14] considered thermal proficiency associated with reciprocating compressor type and with the control system which has steeples capacity. They also built a setup experimental. The results that they presented, the valve clearance and clearance volume Mach number had a negative influence on the thermal proficiency of reciprocating type with the control system which has the stepless capacity.

Using the entropy equation and the exergy concept allows to establish the impact of key factors on the overall irreversibility. The exergy balances allow determining the exergy destruction in various design conditions.

With considering the local exergy losses by Stecco [15], an exergetic efficiency was derived. In this work, the exergy destroyed in the compressor device is attributed to the gas stream warming at the inlet part of a cylinder, the imperfection of the stuffing between the piston and the cylinder and the losses in the input and output valves.

Applying entropy equation and exergy efficiencies in modeling reciprocating compressor is a powerful tool to optimize design factors, consequently, many researchers have applied this concept in their studies [16–18]. In one study, an exergy manner for compressor proficiency detailed examination has been offered by Harte and McGovern [16]. In another study Aprea et al. [18] studied an exergetic lysis of a vapor compressor refrigeration plant, which the refrigeration capacity is controlled by varying the compressor speed. Their results are illustrated that the overall exergetic proficiency of the plant working with R22 is consistently better than that of its substitutes; besides this among the candidate substitutes, in variable speed applications, the best performance is related to the non-izeotropic mixture R407C.

In this current study, a thermodynamic analysis with applying entropy equation was conducted to evaluate the proficiency of reciprocating compressors, which has been compared real gas to ideal one with using ideal state and AGA8 equations respectively in a CNG stations. The main goal was on investigating the influences of various design factors on the compressor irreversibilities. The current finding would be helpful for reducing power consumptions. Furthermore, by modeling this type of compressors, it can be possible to diagnose likely defects which dwindle compressor per-

formance. Angular speed, clearance, pressure ratio and input and output valve areas are included the design parameters. Effects of variations of these design factors on entropy generation, exergy and isentropic efficiencies are explored.

2. Reciprocating compressor process description

In Fig. 1, a schematic picture and kinematics of a classic reciprocating compressor using in CNG stations is shown. The control volume related to compressor is supposed to be the cylinder of compressor, and input and output valves are as spring form. In these compressors, crank-shaft driven by either engine attached to a connecting rod or gas pressure, which it is provided through pressure difference between in-cylinder and suction chamber. It is hypothesized that the gas into control volume to be homogeneous, which means the gas thermal properties are uniform in any part in the cylinder. In the subsequent sections, the governing equations for thermodynamic modeling of the considered compressor are obtained.

3. Thermodynamic modeling

To introduce a numerical model, ideal state equation associated with ideal gas, AGA8 equation related to real gas, continuity equation and subsequently the first and second laws of thermodynamics have been utilized. It is supposed that the interior space of the considered cylinder is control volume so that cylinder boundaries are the wall of cylinder, the cylinder head area and end face of the piston.

3.1. Equations of energy and mass equilibrium

With respect to Fig. 1, the mass balance equation related to the variation rate of the mass inside the cylinder could be described as follows:

$$\dot{m}_c = \dot{m}_s - \dot{m}_d \tag{1}$$

where $\dot{m}_s$ and $\dot{m}_d$ are the rates of mass flow through input and output valves in turn, which are calculating from below equations [19]:

$$\dot{m}_s = \begin{cases} C_{ds}\rho_s A_s \sqrt{\left(\frac{2(P_s - P_{cv})}{\rho_s}\right)} & \text{for } P_s > P_{cv} \text{ and } x_s > 0 \\ -C_{ds}\rho_{cv} A_s \sqrt{\left(\frac{2(P_{cv} - P_s)}{\rho_{cv}}\right)} & \text{for } P_{cv} > P_s \text{ and } x_s > 0 \end{cases} \tag{2}$$

$$\dot{m}_d = \begin{cases} C_{dd}\rho_{cv} A_d \sqrt{\left(\frac{2(P_{cv} - P_d)}{\rho_s}\right)} & \text{for } P_{cv} > P_d \text{ and } x_d > 0 \\ -C_{dd}\rho_d A_d \sqrt{\left(\frac{2(P_d - P_{cv})}{\rho_d}\right)} & \text{for } P_d > P_{cv} \text{ and } x_d > 0 \end{cases} \tag{3}$$

where A_S and A_d are the flow zones through the input and output valves in turn. They could be attained as:

$$A_s = 2\pi x_s r_s, \quad A_d = 2\pi x_d r_d \tag{4}$$

Besides this, x_s and x_d are the input and output motions from the situation which valve is closed in turn, and r_s and r_d are also radius of input and output valves respectively.

Because of non-ideality of valve, when a pressure discrepancy negative is provided from the reference motion of that, the valve does not closed instantaneously. These faults can be counted with using coefficients of C_{dd} and C_{ds}.

The energy balance can be attained as follow equation, of course, with neglecting of potential and kinetic energies [20–22]:

$$\dot{Q}_{cv} + \dot{m}_s h_s = \dot{m}_d h_d + \frac{d}{dt}(mu)_{cv} + \dot{W}_{cv} \tag{5}$$

where $\dot{W}, \dot{Q}, \dot{m}$ and h are work rate, heat transfer, mass flow rates, and enthalpy respectively. Furthermore, cv, d and s subscripts distinguish from control volume, input and output conditions. Work rate of compressor is got by:

$$\dot{W}_{cv} = P_{cv}\frac{dV_{cv}}{dt} \tag{6}$$

In above equation, V and P are volume and pressure in turn.
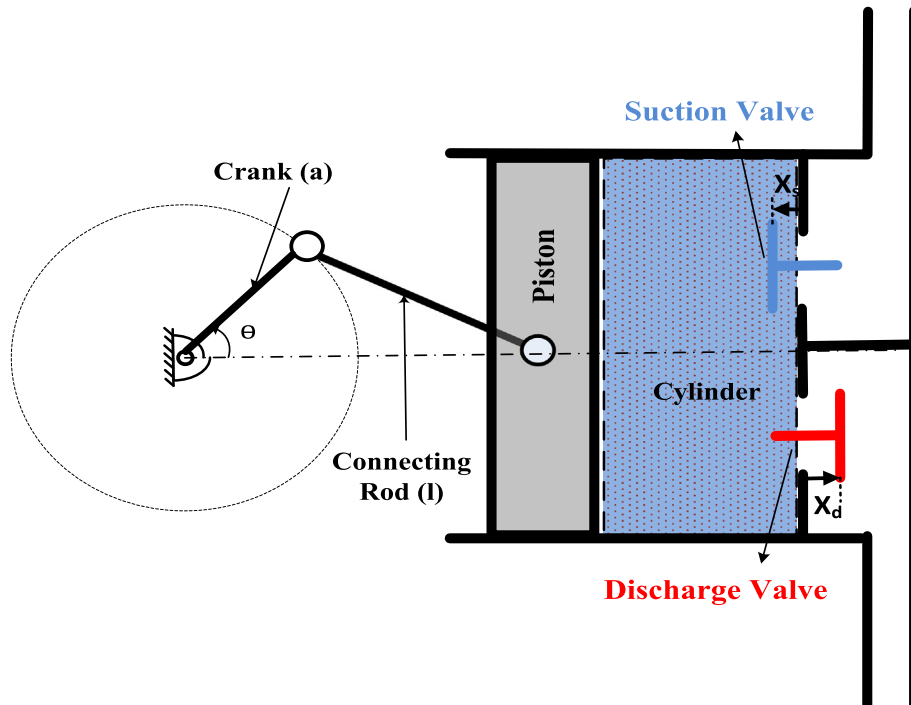
Fig. 1. A Schematic picture of a reciprocating compressor installed in stations.

For converting time to crank angle, it should be differentiated with respect to parameter of time with employing following equation:

$$\frac{d}{dt} = \frac{d}{d\theta} \times \frac{d\theta}{dt} = \omega \frac{d}{d\theta} \qquad (7)$$

where ω is rotational velocity related to the crank shaft and θ is crank angle.

The temporarily cylinder volume during one cycle could be is measured as [19]:

$$V_{cv}(\theta) = A_{cv} \times St(\theta) + V_0 \qquad (8)$$

In this equation, the dead volume is shown with V_0.

The equation that can compute the accurate position in the cylinder which changes with angle related to the crank can be gained as follows [23]:

$$x(\theta) = \frac{St}{2}\left[1 - \cos\theta + \frac{L}{a}\left(1 - \sqrt{\left(1 - \left(\frac{a}{L}\sin\theta\right)^2\right)}\right)\right] \qquad (9)$$

That St is stroke length, L is length of connecting rod and a is length of crank.

Besides this, heat transfer caused by convection in the wall of cylinder can be computed at each moment by below equation:

$$\frac{dQ}{d\theta} = \frac{\alpha A}{\omega}(T_{cv} - T_w) \qquad (10)$$

where A, α, T_w and T_{cv} are surface area, which has direct contact with gas, the coefficient of heat transfer, the temperature which belongs the wall and the in-cylinder temperature of gas in turn. Adair et al. [24] detected that the temperature variation of this wall is fewer than $\pm 1^0 F$, therefore it is presumed that the wall has a constant temperature.

In this work, for calculating convective coefficient of heat transfer (α), the Woschni equation has been utilized [25]. This correlation was originally related to computing heat transfer of internal combustion engine, while it could predict the rate of heat transfer during engine motion compression process. Therefore, this relation could be applied to modeling heat transfer on reciprocating compressors. This relation is stated coefficient of heat transfer by below equation:

$$\alpha = 3.26 D^{-0.2} P^{0.8} T^{-0.55} V_e^{0.8} \qquad (11)$$

That V_e and D are gas characteristic speed and the cylinder diameter in turn. The characteristic speed without part of swirl and for reciprocating compressors can be gained as [25]:

$$V_e = 2.28 V_{eP} \qquad (12)$$

where V_{eP} defines the piston average speed.

3.1.1. Model of ideal gas

The principal equations for the model that gas is assumed ideal could be simplified. In following equation, there are the assumptions related to ideal gas for defining internal energy, enthalpy and gas constant in terms of temperature, pressure and specific heats:

$$u = c_v T, \quad h = c_p T, \quad R = c_p - c_v \qquad (13)$$

By replacing Eqs. (6), (7) and (13) in Eq. (5), the energy balance equation with presuming gas is ideal and for each cycle of reciprocating compressor can be attained as below equation:

$$\frac{dT_c}{d\theta} = \frac{1}{m_c(c_p - R)}\left\{\frac{dQ}{d\theta} + c_p\frac{dm_s}{d\theta}T_s - P_c\frac{dV}{d\theta}\right.$$
$$\left. - c_p\frac{dm_d}{d\theta}T_c - (c_p - R)\left(\frac{dm_s}{d\theta} - \frac{dm_d}{d\theta}\right)T_c\right\} \qquad (14)$$

3.1.2. Model of real gas

When the model of gas is for real one, the energy balance after simplification can be gained as following equation:

$$\frac{du_c}{d\theta} = \frac{1}{m_c}\left\{\frac{dQ}{d\theta} + \frac{dm_s}{d\theta}(h_s - u_c) - \frac{dm_d}{d\theta}(h_d - u_c) - P_c\frac{dV}{d\theta}\right\} \qquad (15)$$

4. Entropy balance

Entropy balance (The second law of thermodynamics) equation in the control volume illustrated in Fig. 1 could be attained as follows [26–28]:

$$\frac{d(ms)_{cv}}{d\theta} = \frac{dm_s}{d\theta}s_s - \frac{dm_d}{d\theta}s_d + \frac{1}{T_0}\frac{\delta Q}{d\theta} + \frac{dS_{gen}}{d\theta} \qquad (16)$$

where s_{cv}, s_s and s_d are entropy on mass units of control volume, input and output respectively. In next parts, the entropy terms related to presuming real gas and ideal one will be introduced.

4.1. Model of ideal gas

It is obvious that the term of $\frac{dm_s}{d\theta}s_s$ is zero, when the input valve is closed. The value of s_s can be got as follows:

$$s_s = c_p \ln\frac{T_s}{T_{ref}} - R\ln\frac{P_s}{P_{ref}} \qquad (17)$$

$T_{ref} = 298.15K$ and $P_{ref} = 101.325kPa$ are supposed as state of reference, and subtitle of 'ref' related to this state. When output valve is open, the term of $\dot{m}_d s_d$ is non-zero, and the value of s_d is gained as:

$$s_d = c_p \ln\frac{T_{cv}}{T_{ref}} - R\ln\frac{P_{cv}}{P_{ref}} \qquad (18)$$

Entropy difference between two moments of crank angle into control volume can be gained as:

$$\frac{d(ms)_{cv}}{d\theta} = \frac{d\left(m_{cv}\left(c_p\ln\frac{T_{cv}}{T_{ref}} - R\ln\frac{P_{cv}}{P_{ref}}\right)\right)}{d\theta} \qquad (19)$$

With replacing the Eqs. (17), (18) and (19) in Eq. (16), entropy generation for each moment of piston movement is attained as:

$$\frac{dS_{gen}}{d\theta} = \frac{d\left(m_{cv}\left(c_p\ln\frac{T_{cv}}{T_{ref}} - R\ln\frac{P_{cv}}{P_{ref}}\right)\right)}{d\theta} + \frac{dm_d}{d\theta}\left(c_p\ln\frac{T_{cv}}{T_{ref}} - R\ln\frac{P_{cv}}{P_{ref}}\right)$$
$$- \frac{dm_s}{d\theta}\left(c_p\ln\frac{T_s}{T_{ref}} - R\ln\frac{P_s}{P_{ref}}\right) - \frac{1}{T_0}\frac{\delta Q}{d\theta} \qquad (20)$$

Eventually total entropy generation for a full cycle for both ideal model and real one is computed as:

$$\frac{dS_{gen}^{(tot)}}{d\theta} = \frac{dS_{gen}^{(1)}}{d\theta} + \frac{dS_{gen}^{(2)}}{d\theta} + \ldots + \frac{dS_{gen}^{(j-1)}}{d\theta} + \frac{dS_{gen}^{(j)}}{d\theta} \qquad (21)$$

5. Computing thermodynamic properties of methane (natural gas)

It is obvious that for attaining in-control volume properties, first it is needed to obtain two thermodynamic properties which are independent, after that properties other properties can be gained. The two properties are internal energy and specific volume (or density), which are calculated from first law of thermodynamic and mass conservation in turn. The manners for calculating thermodynamic properties are offered in this part of study briefly. Farzaneh-Gord et al. [29] deliberated the detailed procedure so as to calculate thermodynamics property.

5.1. AGA8 EOS

The overall procedure of AGA8 EOS can be specified as follows [30]:

$$P = Z\rho_m RT \tag{22}$$

That R, Z and ρ_m are universal constant of gas, compressibility factor and molar density in turn.

In AGA8 manner, compressibility factor can be calculated by utilizing the below equation [30]:

$$Z = 1 + B\rho_m - \rho_r \sum_{n=13}^{18} C_n^* + \sum_{n=13}^{18} C_n^* D_n^* \tag{23}$$

where ρ_r is dwindled density and considered as follows:

$$\rho_r = K^3 \rho_m \tag{24}$$

That in this equation, K is parameter of mixture size that calculates by using subsequent equation [30]:

$$K^5 = \left(\sum_{i=1}^N x_i K_i^{\frac{5}{2}} \right)^2 + 2\sum_{i=1}^{N-1}\sum_{j=i+1}^{N} x_i x_j (K_{ij}^5 - 1)(K_i K_j)^{\frac{5}{2}} \tag{25}$$

In Eq. (25), x_i and x_j are mole fractions of elements i and j in mixture in turn. Besides this, K_i and K_j are size parameters of elements i and j respectively. N and K_{ij} are number of element in gas mixture and binary interaction factor for size respectively.

In Eq. (23), B is coefficient of second virial, and it is defined by the next equation [30]:

$$B = \sum_{n=1}^{18} a_n T^{-u_n} \sum_{i=1}^N \sum_{j=1}^N x_i x_j B_{nij}^* E_{ij}^{u_n} (K_i K_j)^{\frac{3}{2}} \tag{26}$$

where B_{nij}^* and E_{ij} are given by the below equations [30]:

$$B_{nij}^* = (G_{ij} + 1 - g_n)^{g_n}(Q_i Q_j + 1 - q_n)^{q_n}(F_i^{1/2} F_j^{1/2}$$
$$+ 1 - f_n)^{f_n}(S_i S_j + 1 - s_n)^{s_n}(W_i W_j + 1 - w_n)^{w_n} \tag{27}$$

$$E_{ij} = E_{ij}^*(E_i E_j)^{1/2} \tag{28}$$

G_{ij} in Eq. (27), is defined by the below equation [30]:

$$G_{ij} = \frac{G_{ij}^*(G_i + G_j)}{2} \tag{29}$$

The $a_n, f_n, g_n, q_n, s_n, u_n, w_n$ in Eqs. (25)–(29), are state parameters, $E_i, F_i, G_i, K_i, Q_i, S_i, W_i$ are the parameters of corresponding characterization and E_{ij}^*, G_{ij}^* are parameters of corresponding binary interaction.

In Eq. (23), $C_n^*; n = 1, \ldots, 58$ are thermal dependent coefficients which are got by the below equation [30]:

$$C_n^* = a_n(G + 1 - g_n)^{g_n}(Q^2 + 1 - q_n)^{q_n}(F + 1 - f_n)^{f_n} U_n^{u_n} T^{-u_n} \tag{30}$$

In upon equation, parameters of G, F, Q, U are mixture ones and defined as follows [30]:

$$U^5 = \left(\sum_{i=1}^N x_i E_i^{\frac{5}{2}} \right)^2 + 2\sum_{i=1}^{N-1}\sum_{j=i+1}^{N} x_i x_j (U_{ij}^5 - 1)(E_i E_j)^{\frac{5}{2}} \tag{31}$$

$$G = \sum_{i=1}^N x_i G_i + 2\sum_{i=1}^{N-1}\sum_{j=i+1}^{N} x_i x_j (G_{ij}^* - 1)(G_i + G_j) \tag{32}$$

$$Q = \sum_{i=1}^N x_i Q_i \tag{33}$$

$$F = \sum_{i=1}^N x_i^2 F_i \tag{34}$$

That U_{ij} in Eq. (31) is the parameter of binary interaction for mixture energy.

In Eq. (23), D_n^* is considered by the subsequent equation:

$$D_n^* = (b_n - c_n k_n \rho_r^{k_n})\rho_r^{b_n} \exp(-c_n \rho_r^{k_n}) \tag{35}$$

Coefficients of Eq. (35) are gained in Ref. [31].

Replacing Eq. (23) in Eq. (22), the pressure, temperature and natural gas composition are identified. Molar density is the merely unknown parameter. This parameter is computed with using Newton-Raphson iterative method.

After that, the natural gas density is achieved by the below equation:

$$\rho = M_w \rho_m \tag{36}$$

where M_w and ρ_m are mixture molecular weight and molar density respectively. With having molar density value, compressibility factor is attained by using Eq. (29).

Model of AGA8 is considered for specific domain related to the gas components. Table 1 illustrates domain of gas properties that model of AGA8 EOS could be utilized [30]. It illustrates upright proficiency and high precision in the temperature domain between 143.15 K and 676.15 K, and a pressure which is up to 280 MPa.

5.2. Calculating internal energy (u)

If internal energy is considered that is a function of molar specific volume and temperature, so the residual function of internal energy will be intended as [31]:

$$u_m - u_{m,I} = -RT^2 \int_0^{\rho_m} \left(\frac{\partial Z}{\partial T} \right)_{\rho_m} \frac{d\rho_m}{\rho_m} \tag{37}$$

where u_m for real gas specifies internal energy as a molar state, and $u_{m,I}$ for ideal gas identifies molar internal energy. Molar internal energy associated with ideal gas can be attained with using the below equation:

$$u_{m,I} = h_{m,I} - Pv_m = h_{m,I} - RT \tag{38}$$

In Eq. (38), $h_{m,I}$ shows molar enthalpy related to ideal gas and calculated with employing below equation, and T and R are temperature and universal gas constant in turn.

$$h_{m,I} = \sum_{j=1}^N x_j h_{m,i}^j \tag{39}$$

The internal energy per unit mass can be also described as follows:

$$u = \frac{u_m}{M_w} \tag{40}$$

Table 1
Domain of mixture characteristics of gas in AGA8 model [24].

Component (mole%)	Normal domain	Expanded domain
Methane	45–100	0–100
Nitrogen	0–50	0–100
Carbon dioxide	0–30	0–100
Ethane	0–10	0–100
Propane	0–4	0–12
Total butanes	0–1	0–6
Total pentanes	0–0.3	0–4
Hexanes plus	0–0.2	0 to Dew Point
Helium	0–0.2	0–3
Hydrogen	0–10	0–100
Carbon monoxide	0–3	0–3
Argon	0	0–1
Oxygen	0	0–21
Water	0–0.05	0 to Dew Point
Hydrogen sulphide	0–0.02	0–100

5.3. Entropy (s)

Eq. (41) is attained from the Maxwell's relations for describing entropy:

$$\left(\frac{\partial s_m}{\partial v_m}\right)_T = \left(\frac{\partial P}{\partial T}\right)_{v_m} \qquad (41)$$

In this equation, s_m specifies molar entropy. If Eq. (41) is integrated respect to the specific molar volume, and variables are changed, the subsequent equation computing molar entropy can be achieved [31]:

$$s_m = s_{m,I} - R \int_0^{\rho_m} \left[Z + T\left(\frac{\partial Z}{\partial T}\right)_{\rho_m} \right] \frac{d\rho_m}{\rho_m} \qquad (42)$$

In Eq. (42), S_m and $s_{m,I}$ are molar entropy of real model and ideal one in turn. Molar entropy of ideal gas is obtained as follow:

$$s_{m,I} = \sum_{j=1}^N x_j s_{m,i}^j \qquad (43)$$

In Eq. (43), x_j is molar fraction of element j in the mixture, while $s_{m,i}^j$ specifies molar entropy related to ideal gas of element j in the mixture that can be gained as below [31]:

$$s_{m,i}^j(T,P,x_j) = s_{m,i}^j(T) - R\text{Ln}(x_j P) \qquad (44)$$

In Eq. (44), $s_{m,i}^j(T)$ identifies molar entropy related to ideal gas of element j that is a function which changes with varying temperature and explained by below equation [31]:

$$\begin{aligned} s_{m,i}^j(T) = s_{m,i0}^j &+ a_j \text{Ln}(T) \\ &+ b_j \left[\left(\frac{c_j}{T}\right) \coth\left(\frac{c_j}{T}\right) - \text{Ln}\left(\sinh\left(\frac{c_j}{T}\right)\right) \right] \\ &- d_j \left[\left(\frac{e_j}{T}\right) \coth\left(\frac{e_j}{T}\right) - \text{Ln}\left(\cosh\left(\frac{e_j}{T}\right)\right) \right] \end{aligned} \qquad (45)$$

In Eq. (45), $s_{m,i0}^j$ is molar entropy at temperature of reference. The coefficients given in Eq. (45) are presented in Ref. [32]. After that entropy per unit mass can be intended as follows:

$$s = \frac{s_m}{M_w} \qquad (46)$$

6. Algebraic procedure

As described previously, equation of first law and mass conservation equation are discretized so as to compute two thermodynamic properties which are independent [29]. After that for acquiring entropy generation and changing entropy into control volume, the second law is employed. Firstly, these two Eqs. (1) first law and (2) mass conservation can be discretized as below equation: [20–22]

$$\begin{aligned} \frac{u_{c.v}^{j+1} - u_{c.v}^j}{\Delta\theta} = \frac{1}{m_{c.v}^j} &\left\{ \left(\frac{\Delta Q}{\Delta\theta}\right)^j + (h_s^j - u_{c.v}^j)\left(\frac{\Delta m_s}{\Delta\theta}\right)^j \right. \\ &\left. - (h_d^j - u_{c.v}^j)\left(\frac{\Delta m_d}{\Delta\theta}\right)^j - P_{c.v}\left(\frac{\Delta V_{c.v}}{\Delta\theta}\right)^j \right\} \end{aligned} \qquad (47)$$

$$\begin{aligned} \frac{\Delta m_{c.v}}{\Delta\theta} = \frac{\Delta m_s}{\Delta\theta} - \frac{\Delta m_d}{\Delta\theta} &\Rightarrow \frac{m_{c.v}^{j+1} - m_{c.v}^j}{\Delta\theta} = \left(\frac{\Delta m_s}{\Delta\theta}\right)^j - \left(\frac{\Delta m_d}{\Delta\theta}\right)^j \Rightarrow m_{c.v}^{j+1} \\ &= m_{c.v}^j + \Delta\theta\left(\left(\frac{\Delta m_s}{\Delta\theta}\right)^j - \left(\frac{\Delta m_d}{\Delta\theta}\right)^j\right) \end{aligned} \qquad (48)$$

After that $u_{c.v}$ and $m_{c.v}$ are computed from Eqs. (47) and (48) for every crank angle with using Euler's method. Following this, with knowing volume of cylinder at every crank angle, density can be acquired as subsequent equation:

$$\rho_{c.v(\theta)}^{j+1} = \frac{m_{c.v(\theta)}^{j+1}}{V_{c.v(\theta)}^{j+1}} \qquad (49)$$

To identify thermodynamic properties (temperature, pressure …), knowing two thermodynamic properties (density and specific internal energy) are enough. Thermodynamic table, which are created with using AGA8 EOS data, are used for calculating temperature and pressure at each time step. The target table is set according to density (ρ) and internal energy (u). By using Curve fitting method, functions related to temperature and pressure are created. This process is the bases upon the work of Farzaneh-Gord et al. [33]. They expanded exquisite correlations to calculate thermodynamic properties related to natural gas. Their study highlights that the correlations can predict properties associated with natural gas with a mistake which is negligible for lots of engineering applications. The temperature and pressure domains, which the correlations have been expanded for it, are as follows: 0.2 < P (MPa) < 25; 250 < T(K) < 350. The average absolute percent deviation (AAPD) to compute thermodynamic properties related to natural gas according to these temperature and pressure range is fewer than 3%. Detailed calculations of this manner and mistake for curve fitting method exist in Farzaneh-Gord et al. [33].

The second law of thermodynamic for gaining entropy generation, which is discretized, is as below equation [26–28]:

$$\frac{S_{gen}^{j+1} - S_{gen}^j}{\Delta\theta} = \left(\frac{\Delta(ms)_{c.v}}{\Delta\theta}\right)^j - \left(\frac{\Delta m_s}{\Delta\theta}\right)^j s_s^j + \left(\frac{\Delta m_d}{\Delta\theta}\right)^j s_d^j - \frac{1}{T_0}\left(\frac{\Delta Q}{\Delta\theta}\right)^j \qquad (50)$$

With using Euler method, entropy generation at every crank angle is obtained. Of course, knowing other items in this equation in each moment is necessary.

The entropy generation enhances the work required, which is necessary so as to compress the gas into the cylinder. The actual work equals the sum of the area under the P-V and T-S_{gen} diagrams. This amount is also equal to enthalpy difference between inlet and outlet gases from compressor. The actual work of compressor is acquired as following equation [34]:

$$\dot{W}_{ac} = \oint \dot{V}dP - \oint T d\dot{S}_{gen} = \Sigma(\dot{m}_d h_d) - \Sigma(\dot{m}_s h_s) \qquad (51)$$

Exergy efficiency could be also evaluated by [31]:

$$\eta_{ex} = \frac{\Sigma\dot{m}_d Ex_d - \Sigma\dot{m}_s Ex_s}{\dot{W}_{ac}} = \frac{\Sigma\dot{m}_d(h_d - T_0 s_d) - \dot{m}_s(h_s - T_0 s_s)}{\Sigma(\dot{m}_d h_d) - \Sigma(\dot{m}_s h_s)} \qquad (52)$$

That, Ex_d, Ex_s and T_0 are discharge, suction exergy and ambient temperature in turn.

Eventually, isentropic efficiency is obtained as [31]:

$$\eta_{isen} = \frac{\Sigma\dot{m}_d h_{d_s} - \Sigma\dot{m}_s h_s}{\Sigma(\dot{m}_d h_d) - \Sigma(\dot{m}_s h_s)} \qquad (53)$$

where h_{d_s} and T_{d_s} describe discharge enthalpy and discharge temperature in isentropic process respectively.

7. Results

The results for a particular compressor are presented, and methane is presumed as working fluid. Table 2 shows specifications related to the compressor employed in this work for modeling the reciprocating one. The data of geometric features and thermodynamic conditions of that contains in this table. The influences of different factors are also studied in separated sectors.

Table 2
Specifications of the reciprocating CNG compressor used for the model.

Specification	Symbol	Value	Unit
Diameter of Cylinder	D	25	cm
Stroke	S	20.8	cm
Radius of input port	r_s	4.64	cm
Radius of output Port	r_d	8.03	cm
Rotational speed	ω	1200	rpm
Input temperature	T_s	293	K
Output pressure	P_d	15	MPa
Input pressure	P_s	3.75	MPa
Pressure ratio	P_d/P_s	4	–

7.1. Changes of difference terms of entropy with changing clearance

In this sector, the influence of clearance changes on entropy terms related to ideal gas and AGA8 models are presented. The clearances, which are investigated for this study, are 5, 10, 15 and 20%. For these figures, the modeling starts from TDC (Top Dead Center) that cylinder volume in this point is the equal of volume clearance, after that with moving to BDC (Bottom Dead Centre), pressure and consequently other properties of gas into control volume change. The simulation continues until piston comes back again to TDC. Fig. 2 shows entropy changes of input and output terms verse of crank angle and for several clearances and for models of AGA8 and ideal gas. The value of input entropy equals zero until input valve opens. Furthermore, the value of output entropy is non-zero when output valve opens. As regards these figures, as clearance increases, the necessary pressure difference for opening input and output valves are provided later respect to lower clearances, so entropy changes are happened in higher crank angles in the both models. Another interesting point is that entropy changes

of these two terms in AGA8 model are more than ideal one. This difference increases, as clearance grows.

Fig. 3 shows changing entropy terms related to heat transfer (a) and in-control volume (b) verse of crank angle. The figure of entropy diagram associated with heat transfer is like heat transfer diagram, because, consistent with the Eq. (16), this term is reached by dividing heat transfer into ambient temperature. The amounts of heat transfer entropy are really smaller than the amounts of other entropy terms, so this term does not play a prominent role in changing entropy generation. Due to temperature of gas in ideal model during opening output valve is much more than AGA8 one, entropy values related to it are more than AGA8 one. The figure of in-control volume entropy shows that the main changing happens when suction or discharge valve are opening.

In Fig. 4, it is shown changing entropy generation against crank angel for several clearances. It is a principle law that no process is performed, unless entropy generation of that process is positive. This is also true about the considered process. As it can be seen from this picture, the most value of entropy generation is happened when output valve is open, because in this period, temperature of gas is maximum. Another important point is that input and output entropy terms have the most influence on entropy generation.

7.2. Influence of clearance and angular speed on proficiency of compressor for AGA8 and ideal models

The existence of clearance is unavoidable because of various causes for example happening heat expansion in different pieces belong reciprocating compressor. Effects of changing clearances and angular speeds on parameters like entropy generation,
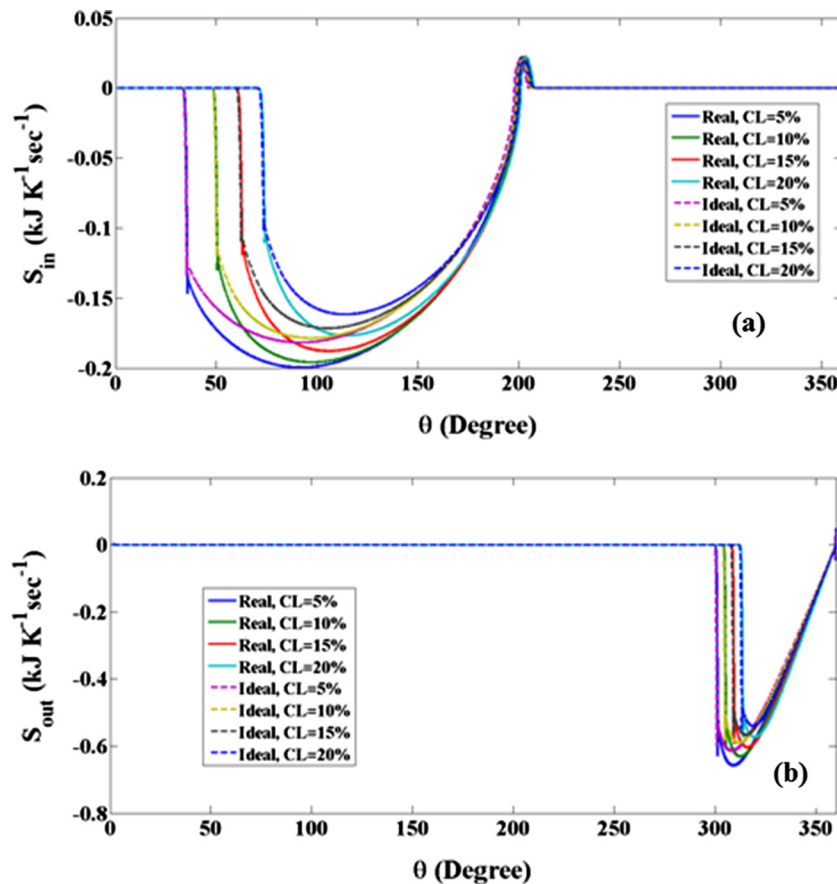
Fig. 2. Entropy changes of the two terms vs. crank angle for several clearances and ideal and AGA8 models including (a) input entropy, (b) output entropy.
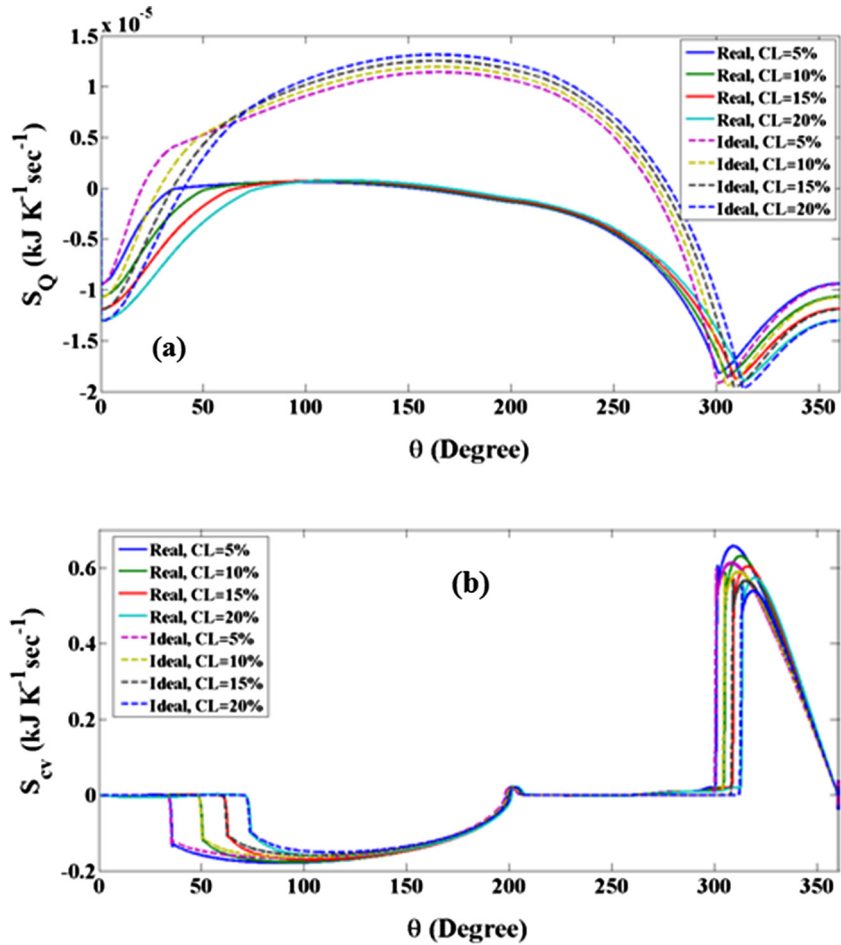
Fig. 3. Entropy changes of the two terms vs. crank angle for several clearances and ideal and AGA8 models including (a) entropy due to heat transfer, (b) entropy of in-control volume.
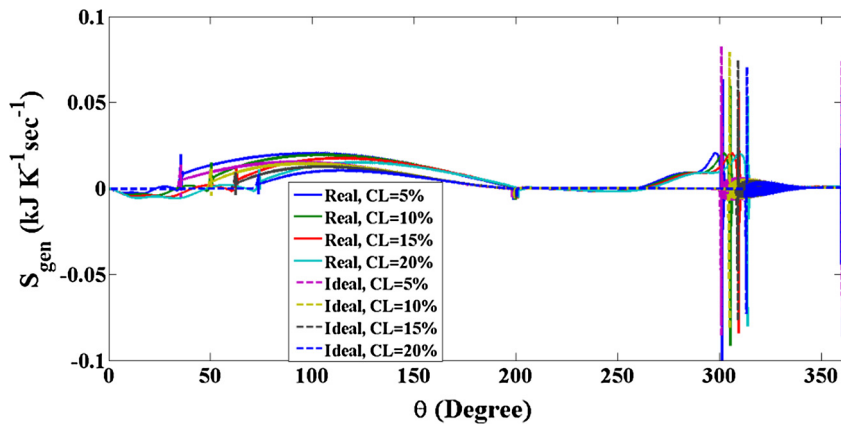
Fig. 4. Entropy generations of compression cycle vs. crank angle for several clearances and for ideal and AGA8 models.

isentropic and exergy efficiencies are investigated in this part of study. Angular speed changes from 1000 to 2500 rpm. Fig. 5 illustrates changes of entropy generation verse to angular speed for different clearances. As it can be seen, with increasing clearances, entropy generation decreases for both ideal and AGA8 models. For instance, entropy generation at ω = 2000 rpm and clearance = 10% is 0.0383 kJ/kg·K, but at ω = 2000 and clearance = 15%, this value equals 0.0295 kJ/kg·K. The reason of that is lower mixing between inlet and remaining gas, which is into dead volume during suction process. Another important point is that entropy genera-

tion increases, when angular speed grows. This phenomenon can be explained in this way that in higher angular speeds, discharge gas temperature increases, so entropy generation increases.

Exergy and isentropic efficiencies diagrams are displayed in Fig. 6 and Fig. 7 respectively. As it can be observed, there is a downward trend in the amounts of both exergy and isentropic efficiencies with increasing angular speed. The cause is that efficiency has an inverse relation with entropy generation. So, increasing clearance improves the efficiencies. It is important to point that due to exergy efficiency is the one which compares work output to
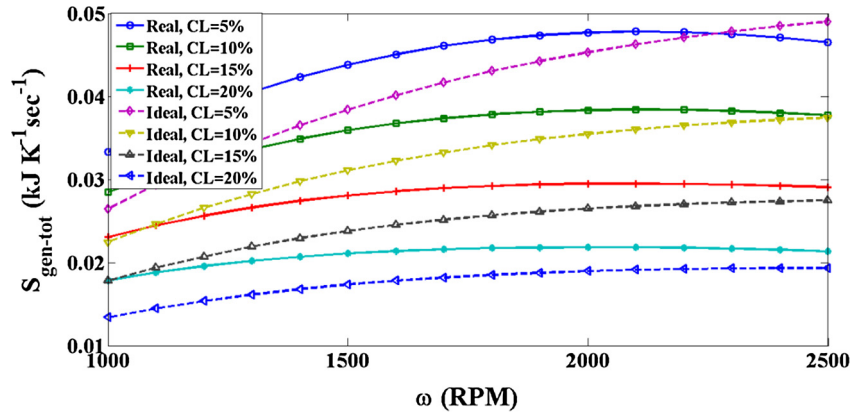
Fig. 5. Variation of entropy generation vs. angular speed for several clearances based upon the ideal and AGA8 models.
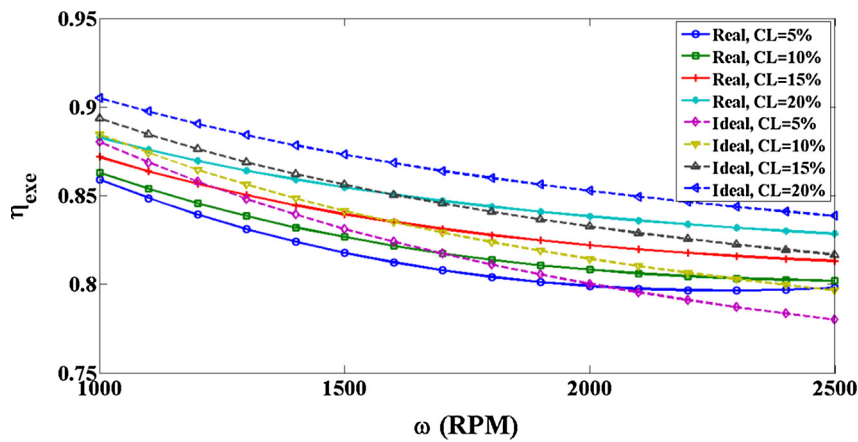
Fig. 6. Variation of exergy efficiency vs. angular speed for several clearances based upon the ideal and AGA8 models.
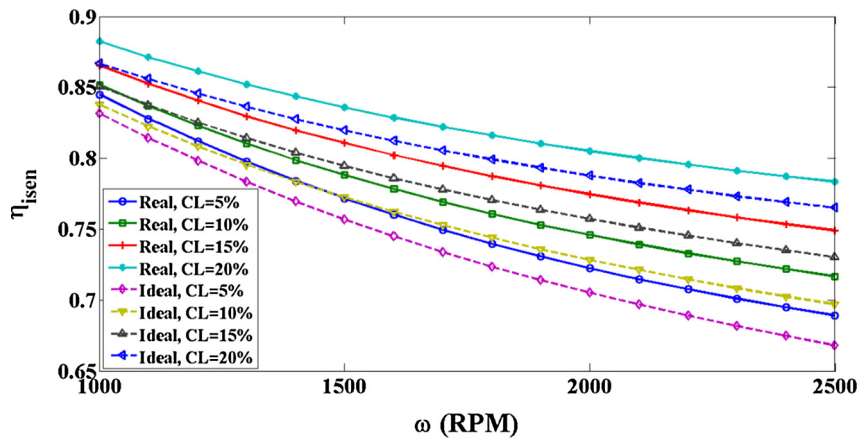
Fig. 7. Variation of isentropic efficiency vs. angular speed for several clearances based upon the ideal and AGA8 models.

the potential of the input to do work, so the value of that is more than isentropic efficiency, which is ideal model, and it compares work output to adiabatic and reversible process. Isentropic efficiency difference between AGA8 and ideal models increases, when angular speed enhances. As the figures present, the trends of ideal model in entropy generation, exergy and isentropic are similar to real gas, but trends of differences between AGA8 and ideal models are not certain. For example, for CL = 5%, difference of entropy generation between AGA8 and ideal models at $\omega = 1000$ rpm is 0.006

(kJ/K·sec), and is 0.0006 (kJ/K·sec) at $\omega = 2200$ rpm, while this difference is 0.003 (kJ/K·sec) at $\omega = 2500$ rpm.

7.3. Influences of changing pressure ratio in diverse angular speeds on compressor proficiency for AGA8 and ideal models

This section intends to illustrate the affect related to pressure ratio and angular speed on performance of compressor for AGA8 and ideal models. In this work, input pressure is constant
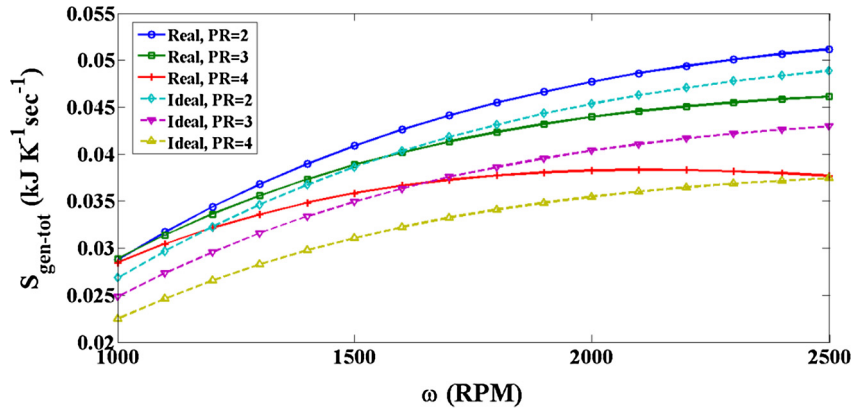
Fig. 8. Variation of entropy generation vs. angular speed for several pressure ratios based upon the ideal and AGA8 models.

(3.75 MPa), and pressure ratios 2, 3 and 4 are considered. Fig. 8 shows changing entropy generation against angular speed for several pressure ratios. As it can be considered, entropy generation increases, when angular speed enhances. Another significant point is that a growth in pressure ratio causes a remarkably decrease in entropy generation. For both AGA8 and ideal models, entropy generation difference between the two pressure ratios increases with rising angular speed, but in AGA8 model, this increase in the value of this difference is more than ideal one.

Figs. 9 and 10 show changing exergy and isentropic efficiencies verse to angular speed for different pressure ratios respectively. As it was explained previously, exergy efficiency has an inverse relation to entropy generation; so, increase in pressure ratio must provide a higher efficiency that it is right about these figures. The amounts of exergy efficiency related to the real model are less than the ideal model, because of having higher entropy generations. The exergy efficiency is 88.5% at pressure ratio = 4 and $\omega = 1000$ rpm for ideal gas, but this amount at that situation is 83.8% for ideal
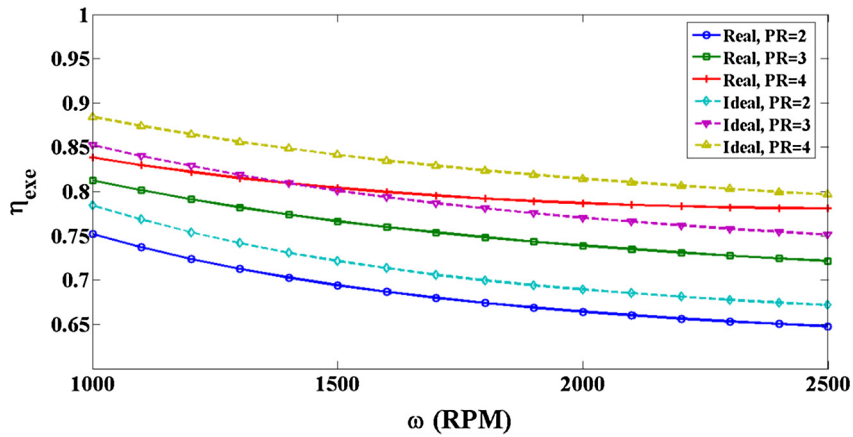
Fig. 9. Variation of exergy efficiency vs. angular speed for several pressure ratios based upon the ideal and AGA8 models.
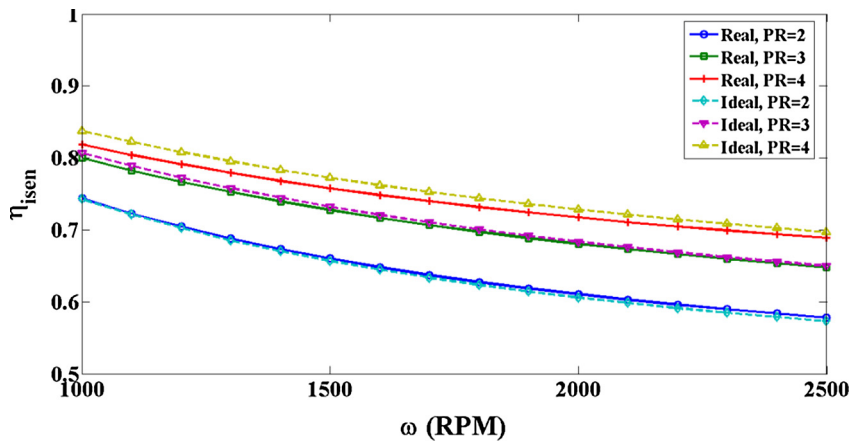
Fig. 10. Variation of isentropic efficiency vs. angular speed for several pressure ratios based upon the ideal and AGA8 models.

gas. This difference of exergy efficiency is 4.7%. The difference of these two models in pressure ratio = 4 and $\omega = 2500$ rpm is 1.4%. Furthermore, the difference between these two models at the pressure ratio = 2 and $\omega = 1000$ rpm is 3%, and at the pressure ratio = 2 and $\omega = 2500$ rpm is 2.4%. So, this difference decreases with increasing angular speed. As it can be realized from fig. 10, with increasing pressure ratio, the difference between the amounts of isentropic efficiency for AGA8 and ideal models enhances.

7.4. Effect of compressor parameters on compressor proficiency for AGA8 and ideal models

In this part, two parameters are introduced: (1) $\beta = \frac{A_d}{A_s}$, which is proportion of output valve area to input valve area, and (2) $\Psi = \frac{A_s + A_d}{A_p}$, which is proportion of the sum of input and output valves areas to piston area of compressor. The domain of these parameters are as follow:

$$0.9 \leqslant \beta \leqslant 3.9; \quad 0.5 \leqslant \Psi \leqslant 0.8$$

It is could be realized later that if Ψ increases, compressor efficiency will increase too, but it cannot be increased from specific value (<0.8) due to manufacturing restriction. For $\beta < 0.9$, the computation method produces unrealistic results and as the aim is to investigate influence β ratio on compressor performance, it is preferred to consider the values which achieve the correct and real results.

Fig. 11 illustrates changes of entropy generation against with β and for different Ψs. For all Ψs, when β increases, entropy generation enhances. It means that with heightening proportion of input valve area to output valve one, entropy generation can decrease, and exergy and isentropic efficiencies can improve (Figs. 12 and 13). For example, instead of choosing $\beta = 3.9$ at $\Psi = 0.5$, if the considered β equals 0.9, exergy efficiency enhances as much as 6.47%. The reason of that is decreasing discharge temperature and subsequently entropy destruction related to lower βs. The ideal model predicts that the amounts of entropy generation and exergy efficiency will be more and less than the predicted amounts of AGA8 model respectively. The difference amount of exergy efficiency between AGA8 and ideal models is 3.9% at $\beta = 0.9$ and $\Psi = 0.5$, while this difference at $\beta = 0.9$ and $\Psi = 0.8$ is 2.32%. So, with increasing Ψ in the lower βs, difference of exergy efficiency between these models will decrease. Besides this, this difference is 1.7% at $\beta = 3.9$ and $\Psi = 0.5$, whereas it is 2.05% at $\beta = 3.9$ and $\Psi = 0.8$. It shows that increase in β decreases the difference value of exergy efficiency between these models, and this difference in the higher β s decreases with increasing Ψ. As it is got from Fig. 13, the amounts of isentropic efficiency attained by the ideal model are less than the real one. Another important point is that difference of these models in computing isentropic efficiency enhances with growing β too. It can be defined that increase in β leading to higher discharge temperature, subsequently increase in entropy generation and decrease in efficiency. So, the ideal model does not predict compressor performance in higher temperatures.
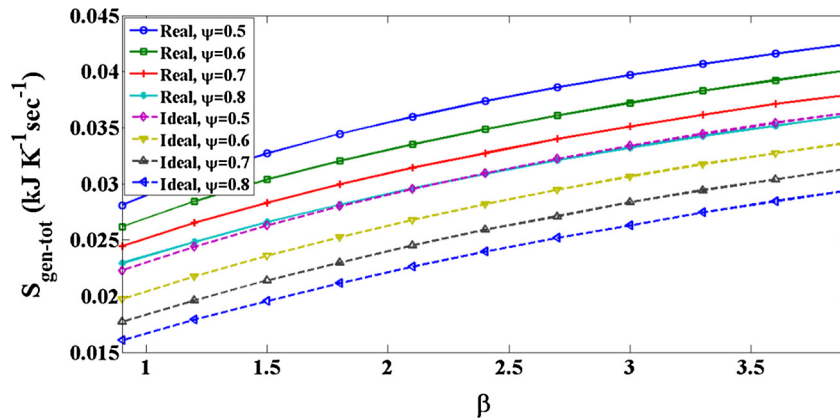
Fig. 11. Variation of entropy generation vs. β for various Ψs based upon the ideal and AGA8 models.
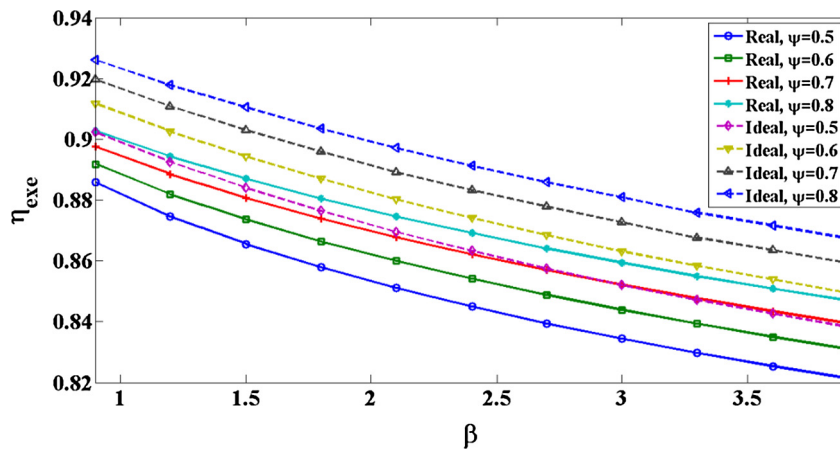
Fig. 12. Variation of exergy efficiency vs. β for various Ψs based upon the ideal and AGA8 models.
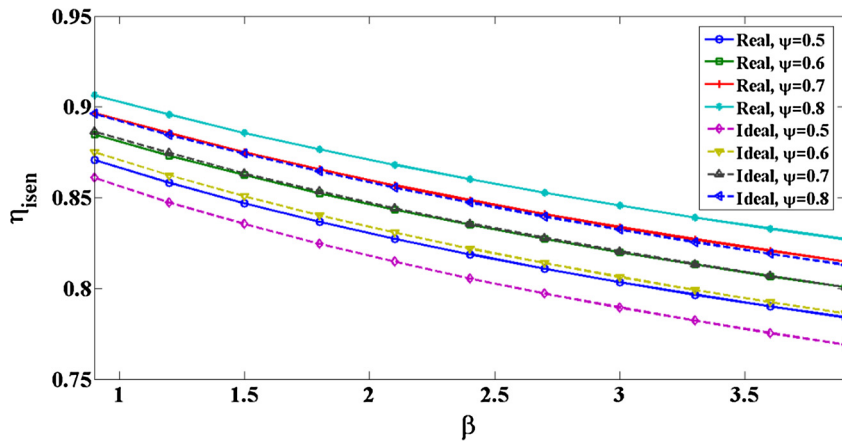
Fig. 13. Variation of isentropic efficiency vs. β for various Ψs based upon the ideal and AGA8 models.

8. Conclusion

Achieving to really high pressure is necessary in industries related to natural gas. One of the main substantial compressor types can be performed for this aim is reciprocating one, and this type has been being applied in CNG stations. For comprehending influences of various factors on compressor behavior, the numerical simulation of different parts of tools is one of the prominent works which have been being applied.

So as to study proficiency of single stage CNG reciprocating compressors, the first and second laws of thermodynamics and equation of mass equilibrium have been applied as theoretic tools. The AGA8 equation of state (EOS) is employed to compute the necessary thermodynamic properties related to natural gas, which methane is presumed as working fluid. The model predicted changing different terms of entropy generation equation like input and output entropies, in-control volume entropy, entropy related to heat transfer and eventually entropy generation against crank angle and for several clearances and with considering ideal and AGA8 models. Furthermore, for these models, the diagrams of total entropy generation for each cycle and exergy and isentropic efficiencies are calculated verse to angular speed and for several clearances, and changing different pressure ratios are also considered. Another work performed in this investigation is introducing two parameters, which are proportional related to areas of piston face, input and output valves, and changing theses parameters for observing compressor performance.

The results illustrate that for both ideal and AGA8 models, with increasing angular speed, entropy generation increases, so exergy and isentropic efficiencies decrease. Moreover, as clearance increases, entropy generation decreases, and it causes exergy and isentropic efficiencies improve. Another significant result is that increase in pressure ratio improves compressor efficiencies. Furthermore, with enhancing proportion of input valve area to output valve area, it can be achievable to acquire a higher efficiency. Difference between AGA8 and ideal models in computing isentropic efficiency for different pressure ratios is relatively negligible, especially in the lower proportions.

References

[1] J. Hu, L. Yang, L. Shao, Ch. Zhang, Generic network modeling of reciprocating compressors, Int. J. Refrig. 45 (2014) 107–119.

[2] M. Farzaneh-Gord, H.R. Rahbari, M. Deymi-Dashtebayaz, Effects of Natural Gas Compositions on CNG Fast Filling Process for Buffer Storage System, 2013, Oil & Gas Science and Technology – Rev. IFP Energies Nouvelles.

[3] M. Farzaneh-Gord, M. Deymi-Dashtebayaz, H.R. Rahbari, Optimising Compressed Natural Gas filling stations reservoir pressure based on thermodynamic analysis, Int. J. Exergy 10 (3) (2012) 299–320.

[4] P. Stouffs, M. Tazerout, P. Wauters, Thermodynamic analysis of reciprocating compressors, Int. J. Thermodyn. Sci. 40 (2000) 52–66.

[5] R. Damle, J. Rigola, J. Castro Perez-Segarra, A. Oliva, Object-oriented simulation of reciprocating compressors: numerical verification and experimental comparison, Int. J. Refrig. 34 (2011) 1989–1998.

[6] M. Farzaneh Gord, A. Niazmand, M. Deymi-DashteBayaz, Optimizing reciprocating air compressor design parameters based on first law analysis, U.P.B. Sci. Bull., Series D, vol. 75, Iss. 4, 2013.

[7] Gord M. Farzaneh, A. Niazmand, M. Deymi-DashteBayaz, H.R. Rahbari, Thermodynamic analysis of natural gas reciprocating compressors based on real and ideal gas models, Int. J. Refrig. 56 (2015) 186–197.

[8] M. Farzaneh Gord, A. Niazmand, M. Deymi-DashteBayaz, H.R. Rahbari, Effects of natural gas compositions on CNG (compressed natural gas) reciprocating compressor performance, J. Energy. 90 (1) (2015) 1152–1162.

[9] E.L. Pereira, C.J. Deschamps, F.A. Ribas, Performance analysis of reciprocating compressors through computational fluid dynamics, Proc. Inst. Mech. Eng. Part J. Process Mech. Eng. 222 (2008) 183–192.

[10] C.D. Pérez-Segarra, J. Rigola, M. Sòria, A. Oliva, Detailed thermodynamic characterization of hermetic reciprocating compressors, Int. J. Refrig. 28 (2005) 579–593.

[11] J. Castaing-Lasvignottes, S. Gibout, Dynamic simulation of reciprocating refrigeration compressors and experimental validation, Int. J. Refrig. 33 (2010) 381–389.

[12] S. Porkhial, B. Khastoo, M.R. Modarres Razavi, Transient characteristic of reciprocating compressors in household refrigerators, Appl. Therm. Eng. 22 (2002) 1391–1402.

[13] C. Aprea, C. Renno, Experimental model of a variable capacity compressor, Int. J. Energy Res. 33 (2009) 29–37.

[14] Tang Bin, Zhao Yuanyang, Li Liansheng, Liu Guangbin, Wang Le, Yang Qicha, et al., Thermal performance analysis of reciprocating compressor with stepless capacity control system, Appl. Therm. Eng. 54 (2013) 380–386.

[15] S.S. Stecco, Exergy analysis of compression and expansion process, Energy 11 (6) (1986) 573–577.

[16] J.A. McGovern, S. Harte, An exergy method for compressor performance analysis, Int. J. Refrig. 18 (6) (1995) 421–433.

[17] C. Aprea, R. Mastrullo, C. Renno, Determination of the compressor optimal working conditions, Appl. Therm. Eng. 29 (2009) 1991–1997.

[18] C. Aprea, F. de Rossi, A. Greco, C. Renno, Refrigeration plant exergetic analysis varying the compressor capacity, Int. J. Energy Res. 27 (2003) 653–669.

[19] J. Brablik, Gas pulsations as a factor affecting operation of automatic valves in reciprocating compressors, in: Proceeding of Purdue compressor Technology Conference, 1972. pp. 188–95.

[20] D. Ndiaye, M. Bernier, Dynamic model of a hermetic reciprocating compressor in on–off cycling operation (abbreviation: compressor dynamic model), Appl. Therm. Eng. 30 (2010) 792–799.

[21] M. Farzaneh-Gord, M. Deymi-Dashtebayaz, H.R. Rahbari, H. Niazmand, Effects of storage types and conditions on compressed hydrogen fuelling stations performance, Int. J. Hydrogen Energy 37 (2012) 3500–3509.

[22] R. Link, C. Deschamps, Numerical modeling of startup and shutdown transients in reciprocating compressors, Int. J. Refrig. 34 (2011) 1398–1414.

[23] Sukhyung Lee, First law analysis of unsteady processes with application to a charging process and a reciprocating compressor. The Ohaio state University: A Thesis presented in Partial Fulfillment of the Requirements for Degree of master Science, 1983.

[24] R.P. Adair, E.B. Qvale, J.T. Pearson, Instantaneous heat transfer to the cylinder wall in reciprocating compressors. Purdue Compressor Technology Conference Proc., 1972, pp 521–526.

[25] Stone Richard, Introduction to Internal Combustion Engines, University of Oxford, Department of Engineering Science, 1999.

[26] A. Bejan, Second-law analysis in heat transfer and thermal design, Adv. Heat Transf. 15 (1982) 1–58.

[27] A. Bejan, Entropy Generation Minimization, CRC, Boca Raton, NY, 1996.

[28] M. Hosseini, I. Dincer, G.F. Naterer, M.A. Rosen, Thermodynamic analysis of filling compressed gaseous hydrogen storage tanks, Int. J. Hydrogen Energy 37 (2012) 5063–5071.

[29] M. Farzaneh-Gord, H.R. Rahbari, Numerical procedures for natural gas accurate thermodynamics properties calculation, J. Eng. Thermophys. 214 (2012) 213e234.

[30] AGA8-DC92 EoS, Compressibility and Super Compressibility for Natural Gas and Other Hydrocarbon Gases. Transmission Measurement Committee, Arlington, VA. Report No. 8, AGACatalog No. XQ 1285, 1992.

[31] M.J. Moran, H.N. Shapiro, Fundamentals of Engineering Thermodynamics, sixth ed., Wiley, ISBN, 2007, p. 0471787353.

[32] J.F. Estela-Uribe J.P.M. Trusler C.R. Chamorro J.J. Segovia M.C. Martin M.A. Villamanan Speeds of sound in {(1_x)CH4 + xN2} with x = (0.10001, 0.19999, and 0.5422) at temperatures between 170 K and 400 K and pressures up to 30 MPa J. Chem. Thermodyn. 38 2006 929 937

[33] Mahmood Farzaneh-Gord, Hamid Reza Rahbari, Developing novel correlations for calculating natural gas thermodynamic properties, Chem. Process Eng. 32 (4) (2011) 435–452.

[34] Richard E. Sonntag, Claus Borgnakke, Gordan J. Van Wylen, 2002. Fundamentals of Thermodynamics, sixth ed., ISBN 13: 9780471152323.